Japanese Journal of Applied Physics **51** (2012) 02BL01 **REGULAR PAPER**
DOI: 10.1143/JJAP.51.02BL01

Complementary Metal–Oxide–Semiconductor Image Sensor with Microchamber Array for Fluorescent Bead Counting

Kiyotaka Sasagawa[1*], Keisuke Ando[1], Takuma Kobayashi[1,3], Toshihiko Noda[1,3], Takashi Tokuda[1,3], Soo Hyeon Kim[2,3], Ryota Iino[2,3], Hiroyuki Noji[2,3], and Jun Ohta[1,3]

[1]*Graduate School of Materials Science, Nara Institute of Science and Technology, Ikoma, Nara 630-0192, Japan*
[2]*Department of Applied Chemistry, The University of Tokyo, Bunkyo, Tokyo 113-8656, Japan*
[3]*JST-CREST, Kawaguchi, Saitama 331-0012, Japan*

Received September 26, 2011; accepted November 11, 2011; published online February 20, 2012

We fabricated a complementary metal–oxide–semiconductor image sensor with a femtoliter microchamber array. The microchamber array plate is used for trapping microbeads and limiting the incident angle of light detected by the sensor. The sensor has an interference filter for fluorescent microbeads imaging. We detected fluorescent and nonfluorescent microbead with this sensor and showed its capability for counting the number of fluorescent chambers. © 2012 The Japan Society of Applied Physics

1. Introduction

Single molecule enzymatic assay is a highly efficient method for measuring ultra-low concentrations of proteins in complex samples.[1–3] This method has been applied for bead-based enzyme-linked immunosorbent assay (ELISA).[4,5] Target molecules are captured by beads with specific antibodies and detected with fluorogenic substrates. By enclosing each bead in a femtoliter chamber and counting the number of beads with fluorescence, low concentrations of proteins can be measured, and even single molecules can be detected.[4,6] This method is applicable for highly sensitive and earlier diagnosis of diseases and infections.

In the conventional system, a fluorescence microscope is used to detect the beads with target molecules, which are captured in the femtoliter chambers. For practical use, a simple and portable system is necessary. We propose to use complementary metal–oxide–semiconductor (CMOS) image sensors for bioimaging.[7–13] Such sensors are suitable for detecting fluorescent beads because they can measure fluorescence and have high-resolution imaging functions. By using such sensors, the system becomes simple and small. In addition, the number of beads observed at one time would be increased owing to the high-definition image sensor, and high throughput would be achieved.

In this work, we fabricated a femtoliter microchamber array on an image sensor. The microchamber array works not only as a chamber for beads but also as a micro optical device to improve imaging characteristics. We demonstrate imaging of fluorescent and nonfluorescent microbeads by using this very compact counting device based on the CMOS image sensor.

2. CMOS Image Sensor with Microchamber Array

Figure 1 shows the structure of the proposed CMOS image sensor with a microchamber array. The chamber array is integrated on a CMOS image sensor for fluorescent imaging. The volume of each cell is femtoliter class. A filter for fluorescent measurement is sandwiched between the microchamber array and the image sensor. Fluorescence imaging is performed by trapping fluorescent and nonfluorescent beads in the chamber array and applying excitation light.

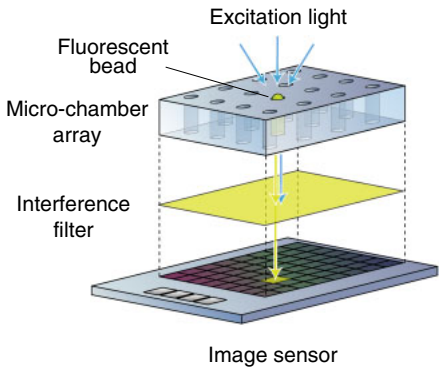

Fig. 1. (Color online) Schematic diagram of CMOS image sensor with microchamber array.

The color filters for standard color image sensors are not sufficient for detecting fluorescence from beads efficiently. Although absorption filters based on dyes are easily coated onto the sensor, their wavelength selectivity is not high. In our previous works, the thickness of the absorption filter layer was from 5 to 90 μm.

In this work, an interference filter was used because the cut-off or cut-on wavelength can be designed to achieve a high extinction ratio. Interference filters are widely used in fluorescence microscopy. However, a disadvantage of this filter is that its transmission spectrum depends on the incident angle of light. Thus, to obtain a high extinction ratio between excitation and fluorescent beams, the excitation light is almost vertically illuminated.

To solve this problem, we propose the use of a Si-based femtoliter chamber array plate based on a high-aspect-ratio hole array we have previously reported.[11] The chamber array plate is a Si plate with a hole array and cuts off the angled incident component. Because the normal incident component of the excitation light can be filtered out by the interference filter, high excitation light rejection is achieved by the combined use of these devices.

Figure 2 and Table I show a micrograph and the specifications of the fabricated sensor module with the chamber array. The sensor was fabricated with a 0.35-μm 2-poly 4-metal standard CMOS technology by austriamicrosystems.

*E-mail address: sasagawa@ms.naist.jp

 © 2012 The Japan Society of Applied Physics

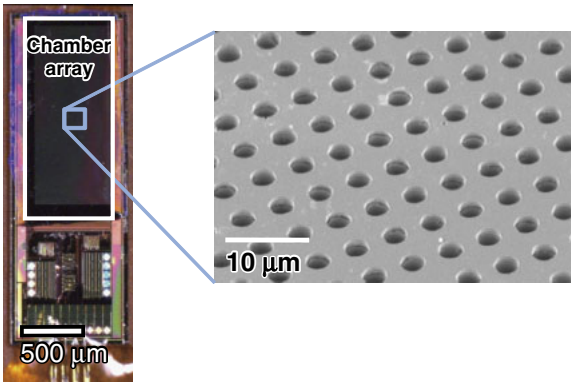

Fig. 2. (Color online) Micrograph of CMOS image sensor module, and scanning electron microscopy image of microchamber array.

Table I. Characteristics of image sensor.

Process		0.35-μm 2-poly 4-metal standard CMOS process
Supply voltage (V)		3.3
Chip size (mm^2)		1.2×3.6
Pixel	Type	3-transistor active pixel sensor
	Size (μm^2)	7.5×7.5
Array size		120×268
Photodiode type		Nwell–Psub
Fill factor (%)		30

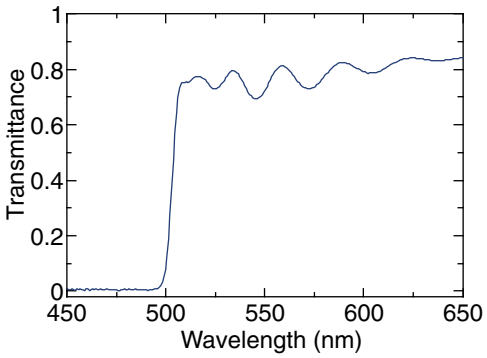

Fig. 3. (Color online) Transmittance spectrum of interference filter.

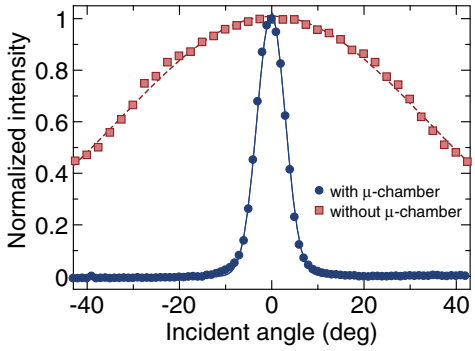

Fig. 4. (Color online) Normalized signal intensities measured with/without microchamber array as functions of incident angle.

The process is as follows. A Si substrate (thickness 60 μm) with an interference filter (cut-on wavelength 500 nm) is bonded on the CMOS image sensor, with the filter side facing the imaging side of the sensor. Amorphous fluoropolymer (CYTOP) is used for the bonding. Next, an Al layer (thickness 200 nm) is deposited by evaporation. The chamber array is patterned on the film by photolithography. After the backside is also coated with an Al layer, the Si substrate is dry etched by deep reactive ion etching (D-RIE), using the patterned Al layer as a mask. The sensor is glued on a polyimide-based flexible printed circuit board and the sensor pads are wire bonded. The bonding wires are covered with epoxy resin for waterproofing and reinforcement.

Figure 2 shows a micrograph of the fabricated sensor module. The diameter of each microchamber hole is approximately 4 μm. The pitch of holes is 15 μm, which is twice that of the pixel array. Thus, there is one hole for every 2×2 pixels.

The transmission spectrum of the interference filter is shown in Fig. 3. The filter is designed to be transparent for light at wavelengths longer than 500 nm. The incident light angle is limited by the microchamber array. To verify this effect, we measured the sensor output as a function of the incident angle. The light source was a halogen lamp, and light at a wavelength of 525 nm was selected by a monochromator. The beam was collimated by a plano-convex lens and launched into the image sensor. Rotating the image sensor controlled the incident angle.

Figure 4 shows the measurement result. The blue circles and red squares are measurements with and without the microchamber array, respectively. The result shows that the incident angle was successfully limited by the microchamber array. The full-width at half maximum with the chamber array is 7.1°. Because the microchamber array is based on Si, it is not perfectly opaque for visible light. Thus, the absorption coefficient decreases as the wavelength increases. However, the result shows that the incident light was effectively suppressed at 525 nm.

Limiting the incident angle improves the spatial resolution when no lens is used for imaging. Moreover, as mentioned above, it is suitable for fluorescent imaging with an interference filter.

3. Imaging of Microbeads Captured by Microchamber Array

Figure 5 shows the experimental setup. In this experiment, commercially available yellow fluorescent beads (Spherotech FP-4052-2) were used to demonstrate the fluorescence imaging capacity of the fabricated sensor module. The absorption and emission peaks were 470 and 485 nm, respectively. The wavelength of fluorescence covers the region from blue-green to red. The fluorescence at a wavelength lower than 500 nm is filtered out by the filter on the sensor, so that the fluorescence is detected by the sensor. The average diameter was 4.1 μm, and the concentration was 0.1% w/v. The suspension was dispersed on the sensor and rinsed with pure water [Fig. 5(a)]. Figure 6 shows a photograph of the microchamber array. Beads were trapped in some chambers. After the imaging experiment, the microbeads were washed out by using a surfactant and the array was rinsed with pure water.

© 2012 The Japan Society of Applied Physics

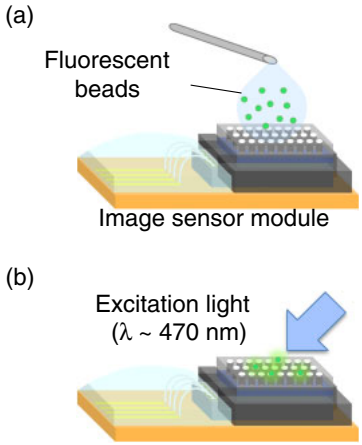

Fig. 5. (Color online) Experimental procedure of fluorescent microbead imaging.

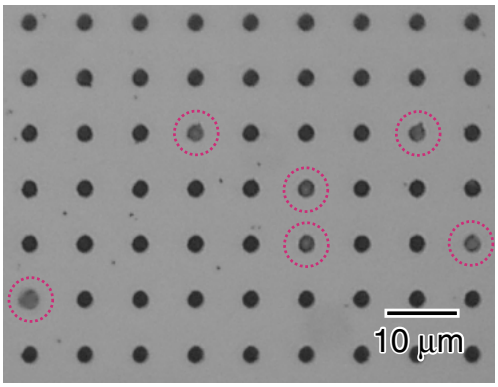

Fig. 6. (Color online) Micrograph of microchamber array. Microbeads are captured in the chambers indicated by the dashed circles.

Figure 7(a) shows the pixel values with and without fluorescent beads. Here, the incident angle of 0° corresponds to the normal incident light. The result indicates a significant difference between the values. This means that the fluorescent beads can be detected by the sensor. The ratio of the pixel values with and without the beads is shown in Fig. 7(b). The highest value is obtained at the incident angle of 30°.

Blue light at wavelengths of 455–490 nm was irradiated to the sensor with an incident angle of 45° [Fig. 5(b)]. The frame rate of the CMOS sensor was set to 2.2 frames per second. The fluorescence microscopy and CMOS sensor images are shown in Figs. 8(a) and 8(b), respectively. For comparison, an overlaid image of Figs. 8(a) and 8(b) is shown in Fig. 8(c). The holes of the chamber array were fabricated at every 4 pixels of the sensor at the intersection points of the vertical and horizontal lines that are guides for the eyes. The yellow points indicate where fluorescent beads are observed in both images. All the red points are on the intersection points of the grid and overlaid with green points, while some green points deviating from the intersection points are not over-laid. These results show that the beads in the holes were successfully and selectively detected with the proposed system.

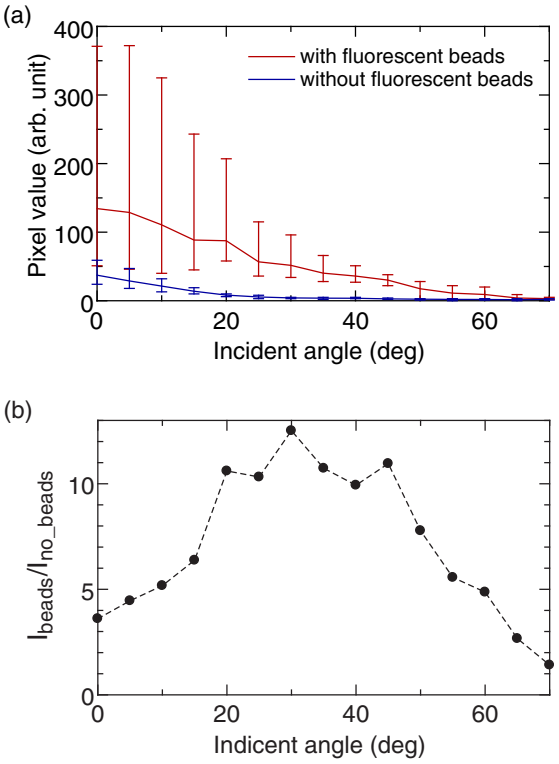

Fig. 7. (Color online) (a) Average values of typical pixels with/without fluorescent beads as functions of incident angle of excitation light. (b) Ratio of average pixel value with fluorescent beads to that without beads.

For digital ELISA measurement, the numbers of fluorescent and nonfluorescent beads are counted and their ratio is calculated. Therefore, it is important to distinguish between filled and empty chambers. Nonfluorescent microbeads (Spherotech PP-30-10) were dispersed on the sensor as well as the fluorescent beads as described above. The sensor was illuminated by green light ($\lambda = 525 \pm 19$ nm) at the incident angle of 45 deg to obtain a bright field image. Here, the filter on the sensor is transparent to the green light. The incident light is filtered out by the microchamber structure without the beads. In the chambers with a bead, the light is scattered by the bead. Some of the scattered light is a vertical incident component and penetrates the microchamber. Thus, the pixel of the chamber filled with a bead indicates higher intensity in comparison with that without any beads.

Figure 9 shows the imaging results. By scattering of the microbeads, the difference between the cells with and without the beads was observed. There is significant correlation between Figs. 9(a) and 9(b). This result indicates that nonfluorescent beads can also be detected with the sensor by bright field illumination.

In this experiment, the aspect ratio of the microchamber array was not optimized and was too high. Thus, the sensitivity of fluorescent detection was low while the full width at half maximum of the incident angle was sufficiently narrow. In this method, the chamber array plate is used for rejection of the excitation light. By reducing the thickness of the plate to the necessary and sufficient condition and optimizing the aspect ratio, the sensitivity would be improved.

© 2012 The Japan Society of Applied Physics

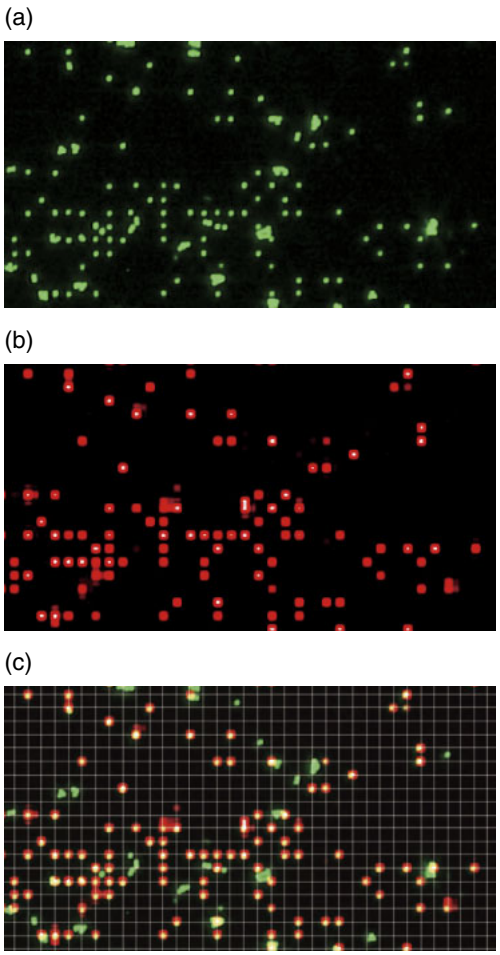

Fig. 8. (Color online) Fluorescent beads images obtained with (a) fluorescence microscopy and (b) CMOS image sensor. (c) Overlaid image.

To verify the principle of microbead detection by the CMOS image sensors integrated with a microchamber array, we used a small image sensor. However, by virtue of the advanced fabrication technology available, fabricating a large image sensor with over 10 M pixels is possible. Thus, a large number of beads could be observable at one time and extremely high throughput could be achieved. This would be a significant advantage of the proposed method.

4. Conclusions

We demonstrated a CMOS image sensor for counting fluorescent beads. By integrating an interference filter and microchamber array plate, the excitation light was successfully filtered out and fluorescent beads were imaged.

On the basis of the proposed method, the number of sensor pixels could be extended by using recent CMOS fabrication processes. This simple detection system can be applied to achieve a portable and high-throughput digital ELISA system.

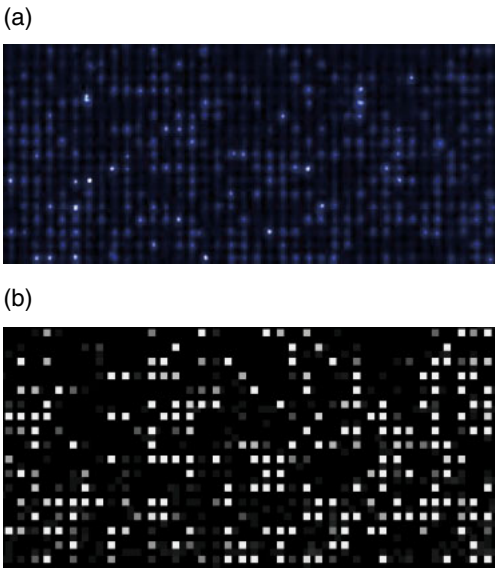

Fig. 9. (Color online) Nonfluorescent beads images obtained with (a) microscope and (b) CMOS image sensor.

Acknowledgments

This work was supported by the Japan Science and Technology Agency, Core Research for Evolutional Science and Technology (JST-CREST) and by VLSI Design and Education Center (VDEC), The University of Tokyo with the collaboration of Cadence Corporation and Mentor Graphics Corporation.

1) Y. Rondelez, G. Tresset, K. V. Tabata, H. Arata, H. Fujita, S. Takeuchi, and H. Noji: Nat. Biotechnol. **23** (2005) 361.
2) S. Sakakihara, S. Araki, R. Iino, and H. Noji: Lab Chip **10** (2010) 3355.
3) D. M. Rissin and D. R. Walt: Nano Lett. **6** (2006) 520.
4) D. M. Rissin, C. W. Kan, T. G. Campbell, S. C. Howes, D. R. Fournier, L. Song, T. Piech, P. P. Patel, L. Chang, A. J. Rivnak, E. P. Ferrell, J. D. Randall, G. K. Provuncher, D. R. Walt, and D. C. Duffy: Nat. Biotechnol. **28** (2010) 595.
5) D. M. Rissin, D. R. Fournier, T. Piech, C. W. Kan, T. G. Campbell, L. Song, L. Chang, A. J. Rivnak, P. P. Patel, G. K. Provuncher, E. P. Ferrell, S. C. Howes, B. A. Pink, K. A. Minnehan, D. H. Wilson, and D. C. Duffy: Anal. Chem. **83** (2011) 2279.
6) E. A. Ottesen, J. W. Hong, S. R. Quake, and J. R. Leadbetter: Science **314** (2006) 1464.
7) J. Ohta, T. Tokuda, K. Sasagawa, and T. Noda: Sensors **9** (2009) 9073.
8) J. Ohta, T. Kobayashi, T. Noda, K. Sasagawa, and T. Tokuda: IEICE Trans. Commun. **E94-B** (2011) 2454.
9) A. Tagawa, M. Mitani, H. Minami, T. Noda, K. Sasagawa, T. Tokuda, and J. Ohta: Jpn. J. Appl. Phys. **49** (2010) 04DL02.
10) T. Kobayashi, A. Tagawa, T. Noda, K. Sasagawa, T. Tokuda, Y. Hatanaka, H. Tamura, Y. Ishikawa, S. Shiosaka, and J. Ohta: Jpn. J. Appl. Phys. **49** (2010) 117001.
11) K. Sasagawa, M. Mitani, T. Sugiyama, T. Noda, T. Tokuda, and J. Ohta: Jpn. J. Appl. Phys. **49** (2010) 04DL03.
12) D. C. Ng, T. Nakagawa, T. Mizuno, T. Tokuda, M. Nunoshita, H. Tamura, Y. Ishikawa, S. Shiosaka, and J. Ohta: IEEE Sens. J. **8** (2008) 121.
13) H. Tamura, D. C. Ng, T. Tokuda, H. Naoki, T. Nakagawa, T. Mizuno, Y. Hatanaka, Y. Ishikawa, J. Ohta, and S. Shiosaka: J. Neurosci. Methods **173** (2008) 114.

© 2012 The Japan Society of Applied Physics